

9-13-2012

Alternative characterization of the spherical to axially deformed shape-phase transition in the interacting boson model

L. R. Dai
Liaoning Normal University

F. Pan
Liaoning Normal University

L. Liu
Liaoning Normal University

L. X. Wang
Liaoning Normal University

J. P. Draayer
Louisiana State University

Follow this and additional works at: https://repository.lsu.edu/physics_astronomy_pubs

Recommended Citation

Dai, L., Pan, F., Liu, L., Wang, L., & Draayer, J. (2012). Alternative characterization of the spherical to axially deformed shape-phase transition in the interacting boson model. *Physical Review C - Nuclear Physics*, 86 (3) <https://doi.org/10.1103/PhysRevC.86.034316>

This Article is brought to you for free and open access by the Department of Physics & Astronomy at LSU Scholarly Repository. It has been accepted for inclusion in Faculty Publications by an authorized administrator of LSU Scholarly Repository. For more information, please contact ir@lsu.edu.



CHORUS

This is the accepted manuscript made available via CHORUS. The article has been published as:

Alternative characterization of the spherical to axially deformed shape-phase transition in the interacting boson model

L. R. Dai, F. Pan, L. Liu, L. X. Wang, and J. P. Draayer

Phys. Rev. C **86**, 034316 — Published 13 September 2012

DOI: [10.1103/PhysRevC.86.034316](https://doi.org/10.1103/PhysRevC.86.034316)

Alternative characterization of the spherical to axially deformed shape-phase transition in the interacting boson model

L. R. Dai,^{1,2} F. Pan*,^{1,3} L. Liu,¹ L. X. Wang,¹ and J. P. Draayer³

¹*Department of Physics, Liaoning Normal University, Dalian 116029, China*

²*Kavli Institute for Theoretical Physics China, CAS, Beijing 100190, China*

³*Department of Physics and Astronomy, Louisiana State University, Baton Rouge, LA 70803-4001, USA*

(Dated: September 3, 2012)

The quantum phase transitional behavior of an alternative characterization of the spherical to axially deformed shape-phase transition in the interacting boson model is explored. Specifically, the usual $SU(3)$ quadrupole-quadrupole interaction is replaced by an $O(6)$ cubic interaction, and the transitional behavior of the low-lying energy levels, eigenstates, isomer shifts, E2 transition rates, and expectation values of shape variables across the entire transitional region are all examined within this context. A comparison with outcomes of the usual $U(5)$ - $SU(3)$ transitional description shows that the spherical to axially deformed shape-phase transition can also be described within this alternative context, especially near the critical point. However, with the $O(6)$ cubic interaction the transition is considerably smoother than for the $U(5)$ - $SU(3)$ case, but with the nuclear shape less well defined, even in the axially deformed limit. It is also shown that the new scheme seems better than the usual $U(5)$ - $SU(3)$ scheme in describing low-lying spectrum of ^{152}Sm with the $X(5)$ critical point symmetry.

PACS numbers: 21.10.Ky; 21.10.Re; 21.60.Fw

I. INTRODUCTION

The nature of quantum shape-phase transitions in finite many-body systems is important in understanding their dynamical behavior [1–4]. In the interacting boson model (IBM) for nuclei, it is now widely accepted that the three limiting cases [5–7] of the theory correspond to three different geometric shapes of nuclei, referred to as spherical (vibrational limit with $U(5)$ symmetry), axially deformed (rotational limit with $SU(3)$ symmetry), and γ -soft (triaxial with $O(6)$ symmetry), respectively. The full range of the model can be parameterized in terms of the Casten triangle [8]. Interesting phenomena occur when a system falls between two limits of the theory, in which case a quantum phase transition occurs at a critical point [9–11] where the dominance of one of the symmetries yields to the dominance of the other. And indeed, the $U(5)$ - $SU(3)$ transitional description for Nd, Sm, Gd, and Dy was first reported in [12]. Later on, the $X(5)$ symmetry at the critical point of this transition was studied [13], in which Iachello proposed analytical solutions of a Bohr Hamiltonian in the situation appropriate for the description of nuclei near the critical point of the spherical to axially deformed shape-phase transition. Casten and Zamfir showed in [14] that ^{152}Sm and other $N = 90$ isotones demonstrate these characteristics.

Transitional patterns from the spherical, $U(5)$, to the axially deformed, $SU(3)$, limit of the IBM with a schematic Hamiltonian were studied in [15–17]; in particular, the transitional behavior of some physically relevant quantities across the entire span of the $U(5)$ - $SU(3)$ transitional region were explored. In present work, the quantum phase transitional behavior for an alternative characterization of the spherical to axially deformed shape-phase transition is analyzed, one where the well-known $SU(3)$ quadrupole-quadrupole interaction in the schematic Hamiltonian of the $U(5)$ - $SU(3)$ description is replaced by the $O(6)$ $[\hat{Q}(0) \times \hat{Q}(0) \times \hat{Q}(0)]^0$ cubic interaction, where $\hat{Q}_\mu(0) = s^\dagger \tilde{d}_\mu + d_\mu^\dagger s$ are generators of the $O(6)$ algebra. This idea was first suggested by van Isacker [18] and then further studied by Thiamova and Cejnar [19]. From these investigations one understands that similar results can be realized when the quadratic scalar formed with the $U(5)$ - $SU(3)$ quadrupole operator is replaced by the cubic scalar formed with the quadrupole interaction of the $O(6)$ limit. The purpose of the present study is to investigate transitional patterns in the latter scheme and to compare them with those of the original $U(5)$ - $SU(3)$ description. In the following, the new scheme will be called the UQ scheme.

To compare the shape-phase transitional behavior in the UQ scheme with those in the $U(5)$ - $SU(3)$ scheme, we will study transitional patterns of some physical quantities, such as low-lying energy levels, eigenstates, isomer shifts, $E2$ transition rates, and some related quantities across the entire transitional region in both schemes. We will show that many typical quantities in the new scheme indeed display almost the same transitional patterns as found in the original $U(5)$ - $SU(3)$ description, especially near the critical point. The analysis further confirms that the $O(6)$ cubic interaction plays a role similar to that of the $SU(3)$ quadrupole-quadrupole interaction in the entire transitional region. However, there are still some quite noticeable differences between the two schemes, which will be shown in Sec. II and III.

II. HAMILTONIAN

It is well known that the consistent- Q Hamiltonian [20] can be used to describe the most general situation in the IBM, which is given by

$$\hat{H}_Q = c_1 \left[x \hat{n}_d + \frac{x-1}{f_1(N)} \hat{Q}(\chi) \cdot \hat{Q}(\chi) \right], \quad (1)$$

where N is the total number of bosons, \hat{n}_d is the number operator for counting d -bosons, $\hat{Q}_\mu(\chi) = (d^\dagger s + s^\dagger \tilde{d})_\mu^{(2)} + \chi (d^\dagger \tilde{d})_\mu^{(2)}$, x and χ are control parameters, $f_1(N)$ is a linear function of N , and c_1 is the scaling factor. Therefore, three limit situations of the model are given by $x = 1$ for the $U(5)$, $x = 0$ and $\chi = 0$ for the $O(6)$, and $x = 0$ and $\chi = -\frac{\sqrt{7}}{2}$ for the $SU(3)$, respectively. On the other hand, van Isacker showed in [18] that a spectrum generated by the $O(6)$ $[\hat{Q}(0) \times \hat{Q}(0) \times \hat{Q}(0)]^0$ cubic interaction, in which $\hat{Q}_\mu(0) = s^\dagger \tilde{d}_\mu + d_\mu^\dagger s$ are the $O(6)$ quadrupole operators, has all the features of a deformed nucleus. As shown in [18], the spectrum generated by $[\hat{Q}(0) \times \hat{Q}(0) \times \hat{Q}(0)]^0$ is one of γ vibrations (i.e., quadrupole vibrations around a spheroidal equilibrium shape that break axial symmetry) with rotational bands built on each vibration, which describes an axially deformed situation despite $\chi = 0$ in this case, though the phenomenological background is still unclear at the moment. Therefore, instead of the consistent- Q Hamiltonian (1), one may consider the following alternative Hamiltonian to describe the most general situation in the IBM:

$$\hat{H}_A = c_2 \left[y\hat{n}_d + \frac{(y-1)t}{f_1(N)}\hat{Q}(0) \cdot \hat{Q}(0) + \frac{(1-y)(1-t)}{f_2(N)}[\hat{Q}(0) \times \hat{Q}(0) \times \hat{Q}(0)]^0 \right], \quad (2)$$

where the parameter $c_2 > 0$, y and t are the control parameters of the new scheme with $0 \leq y, t \leq 1$, and $f_2(N)$ is a quadratic function of N . The linear and quadratic nature of $f_1(N)$ and $f_2(N)$ with N , respectively, ensures that the two terms in (1) or three terms in (2) scale with number of bosons N in a similar way. It can be clearly seen that not only the usual one- and two-body interactions, but also the $O(6)$ three-body term used to describe axially deformed shape phase are included in (2). In the deformed limit, in addition to the three-body $[\hat{Q}(0) \times \hat{Q}(0) \times \hat{Q}(0)]^0$ term, other two-body terms constructed from a linear combination of the $O(3)$ Casimir operator and $O(3)$ scalars of the $O(5)$ generators may also be included as shown in [19], which are not considered in this work for simplicity because the three-body $[\hat{Q}(0) \times \hat{Q}(0) \times \hat{Q}(0)]^0$ term in (2) plays the role similar to the two-body $\hat{Q}(-\sqrt{7}/2) \cdot \hat{Q}(-\sqrt{7}/2)$ term in the consistent- Q formalism (1), where $\hat{Q}_\mu(-\sqrt{7}/2) = (s^\dagger \tilde{d}_\mu + d_\mu^\dagger s) - \sqrt{7}/2(d^\dagger \tilde{d})_\mu^{(2)}$ are the $SU(3)$ generators.

Thus, in the $U(5)$ - $SU(3)$ scheme [15], the Hamiltonian is given by

$$\hat{H}_1 = c_1 \left[x\hat{n}_d + \frac{(x-1)}{f_1(N)}\hat{Q}(-\sqrt{7}/2) \cdot \hat{Q}(-\sqrt{7}/2) \right], \quad (3)$$

which is the special case of the consistent- Q formalism (1) suitable to describe the spherical to axially deformed shape phase transition. As shown in [13, 15, 21], the critical point x_c will be different for different choices of the function $f_1(N)$. In the following, we adopt $f_1(N) = 4N$ as used in [13, 15, 21].

Alternatively, in the UQ scheme, which is the special situation in the alternative scheme (2) with $t = 0$, and also suitable to describe the same shape phase transition in this region, the Hamiltonian is given by

$$\hat{H}_2 = c_2 \left[y\hat{n}_d + \frac{(1-y)}{f_2(N)}[Q(0) \times Q(0) \times Q(0)]^0 \right]. \quad (4)$$

In this case we use $f_2(N) = 0.8N^2$, which puts the critical point y_c of the UQ scheme close to x_c of the $U(5)$ - $SU(3)$ scheme.

In order to diagonalize Hamiltonians (3) and (4), we expand the corresponding eigenstates in terms of the $U(6) \supset SU(3) \supset SO(3)$ basis vectors $|N(\lambda\mu)KL\rangle$ as

$$|NL\xi\rangle = \sum_{(\lambda\mu)K} C_{(\lambda\mu)K}^{L\xi} |N(\lambda\mu)KL\rangle, \quad (5)$$

where ξ is used to denote the ξ -th level with angular momentum quantum number L , and the $C_{(\lambda\mu)K}^{L\xi}$ are expansion coefficients. Since the total number of bosons N is fixed for a given nucleus, the eigenstates given in (5) will also be denoted as $|L\xi; z\rangle$ with $z = x$ for the $U(5)$ - $SU(3)$ scheme or $z = y$ for the UQ scheme in the following, where the value of the control parameter z is explicitly shown. In our calculations, the orthonormalization process [22, 23] with respect to the additional quantum number K needed to label the basis vectors of $SU(3) \supset SO(3)$ and the phase convention for the $U(6) \supset SU(3)$ basis vectors proposed in [24] are adopted. By using analytic expressions for $U(6) \supset SU(3)$ reduced matrix elements of the d -boson creation or annihilation operator [24] and an algorithm [22, 23] for generating the $SU(3) \supset SO(3)$ Wigner coefficients, the eigenequation that simultaneously determines the eigenenergy and the corresponding set of the expansion coefficients $C_{(\lambda\mu)K}^{L\xi}$ can be established, with results that can then be used to calculate physical quantities in both schemes.

III. RESULTS AND DISCUSSIONS

In order to investigate the shape-phase transitional behavior of both schemes, we fixed the total number of bosons at $N = 10$ if not specified and allowed the control parameter x or y to vary in the closed interval $x \in [0, 1]$ or $y \in [0, 1]$. In the following, we present the calculated results in both $U(5)$ - $SU(3)$ and UQ schemes, including some low-lying energy levels and ratios, the $SU(3)$ amplitudes in the ground state and overlap of the ground state and typical overlap of two excited states, the isomer shifts, E2 transition rates, expectation values of the shape variables, and some other relevant quantities.

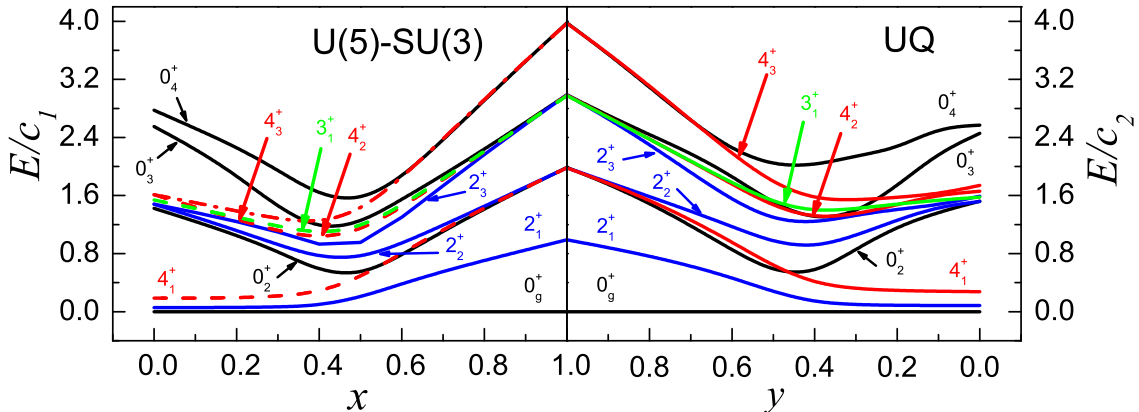


FIG. 1: (Color online) Some low-lying energy levels as function of the control parameter x for the $U(5)$ - $SU(3)$ scheme and y for the UQ scheme.

A. Energy levels

In Fig. 1, some low-lying energy levels as functions of the control parameter in both the $U(5)$ - $SU(3)$ and UQ schemes are shown. One can see that there is a minimum in the excitation energy both in the $U(5)$ - $SU(3)$ scheme and in the UQ scheme except 2_1^+ and 4_1^+ levels. In the $U(5)$ - $SU(3)$ scheme the minimum is around $x \sim 0.41 - 0.47$, while in the UQ scheme it is around $y \sim 0.41 - 0.48$. The minimum in both schemes is all within the spherical to axially deformed shape coexistence region referred to as the critical region. It can also be seen that the minima in different excited levels are not exactly at the same point in the $U(5)$ - $SU(3)$ and UQ schemes, but all fall within the corresponding critical region of the spherical to axially deformed shape-phase transition. Most importantly, the energy valley formed on the critical point in the UQ scheme is shallower than that in the $U(5)$ - $SU(3)$ scheme, especially in higher excited levels, as shown in Fig. 1. Though our calculation was carried out for a single finite N case only, one can deduce from the results that the quantum phase transition in the UQ scheme is smoothed due to the replacement of the $SU(3)$ quadrupole-quadrupole interaction by the $O(6)$ cubic interaction, and as shown below, this smoothed transitional behavior in the UQ scheme also emerges in other quantities.

B. Energy ratios

Two energy ratios, $R_{02} = E_{0_2^+}/E_{2_2^+}$ and $R_{42} = E_{4_2^+}/E_{2_2^+}$ for both the $U(5)$ - $SU(3)$ and the UQ schemes are shown in Fig. 2. With $N = 10$ shown by the solid line in Fig. 2 for example, the ratio R_{02} in the $U(5)$ - $SU(3)$ scheme drops precipitously from the rotational limit $R_{02} \sim 25$ to the vibrational value with $R_{02} \sim 2$ near the critical point, while the ratio R_{02} in the UQ scheme gradually drops from the rotational limit with $R_{02} \sim 18$ to the vibrational value with $R_{02} \sim 2$. The vibrational value, $R_{02} \sim 2$, remains unchanged when x or y is greater than the corresponding critical point value. The ratio R_{42} in both the $U(5)$ - $SU(3)$ and the UQ schemes drops dramatically across the critical region from the rotational limit $R_{42} \sim 3.3$ to the vibrational limit $R_{42} = 2$, with the sharpest change around the critical point with $x_c \sim 0.47$ in the $U(5)$ - $SU(3)$ scheme or $y_c \sim 0.48$ in the UQ scheme. Most noticeably, all the ratios keep to be constant when $x \geq x_c$ in the $U(5)$ - $SU(3)$ scheme or $y \geq y_c$ in the UQ scheme, which confirms that the quasidynamical $U(5)$ symmetry introduced in [25, 26] emerges in this case.

C. Eigenstates

To show how the transition occurs in the ground state for the $U(5)$ - $SU(3)$ and UQ schemes, the amplitudes $|C_{(\lambda,\mu)}|^2$ for each are plotted as functions of the control parameter x and y in Fig. 3, which indicate that the most rapid change in these amplitudes also occurs within the critical region. Differences in the changes of the amplitudes $|C_{(\lambda,\mu)}|^2$ with a variation of the control parameter x or y in the two schemes are noticeable. Specifically, with

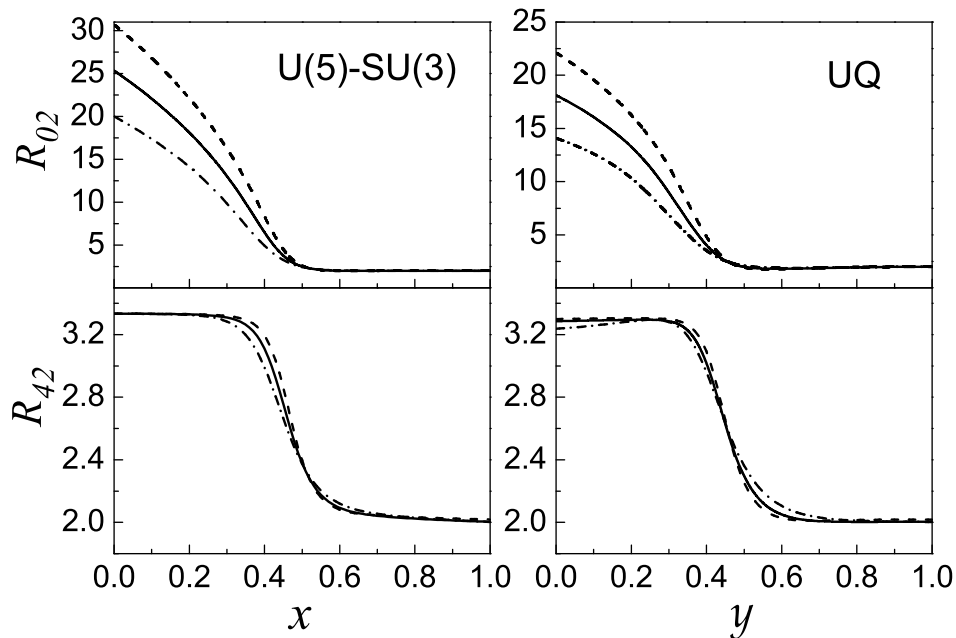


FIG. 2: Energy ratios R_{02} and R_{42} as functions of the control parameter x for the $U(5)$ - $SU(3)$ scheme and y for the UQ scheme, where the dash-dotted line, solid line, and dashed line show the results of $N = 8, 10, 12$, respectively.

increasing value of the control parameter, the $|C_{(2N,0)}|^2$ component decreases more drastically in the $U(5)$ - $SU(3)$ scheme than for the UQ scheme; the $|C_{(2N-6,0)}|^2$ component is less important in the $U(5)$ - $SU(3)$ scheme, while it becomes non-negligible when $y < y_c$ with a sharp change near the critical point in the UQ scheme.

Next, in order to show how the position of the critical point changes with different choices for the function $f_1(N)$ in the $U(5)$ - $SU(3)$ scheme and $f_2(N)$ in the UQ scheme, overlaps $|\langle 0_g^+; z | 0_g^+; z_0 \rangle|$ with $z_0 = 0$ or 1 in the two schemes were calculated. In the upper panel of Fig. 4, the overlaps for different choices of $f_1(N)$ with $f_1(N) = 0.5N, 2N, 4N$, and $8N$, respectively, are shown. It can be clearly seen that the position of the critical (crossing) point changes with different choices of the function $f_1(N)$. The larger the $f_1(N)$ value, the smaller the critical point x_c . Similar behavior also emerges in the UQ scheme as shown in the lower panel of Fig. 4 where the overlaps with $f_2(N) = 0.1N^2, 0.5N^2, 0.8N^2$, and $2N^2$, respectively, are plotted.

It should also be pointed out that the critical point may differ from one excited state to the other for the same choice of $f_1(N)$ or $f_2(N)$ in the two schemes. Our results show that the positions of the critical point in $0_g^+, 2_1^+$, and 4_1^+ states are almost the same, but they are somewhat different in 2_3^+ and 3_1^+ states in the two schemes.

It should also be noted that curves of the overlaps $|\langle L_\xi^+; z | L_\xi^+; z_0 \rangle|$ with $z_0 = 0$ or 1 even become irregular in the $0_2^+, 2_2^+, 4_2^+$, and 0_3^+ states in both schemes. Typical examples of these curves for higher excited states are shown in Fig. 5, which indicate that not only the positions of the critical point in higher excited states may be quite different from that in the ground state, but also the first derivative of $|\langle L_\xi^+; z | L_\xi^+; z_0 \rangle|$ with $z_0 = 0$ or 1 may be discontinuous. For example, the first derivative of $|\langle L_\xi^+; x | L_\xi^+; x_0 \rangle|$ with $x_0 = 0$ or 1 is discontinuous at $x \sim 0.35$ or $x \sim 0.4$ in the $U(5)$ - $SU(3)$ scheme, while $|\langle L_\xi^+; y | L_\xi^+; y_0 \rangle|$ with $y_0 = 0$ or 1 is discontinuous at $y \sim 0.38$ or $y \sim 0.3$ in the UQ scheme. The emerging irregularity manifests that the critical points of the shape phase transition in higher excited states are different from that in the ground state, which is mainly due to the level crossing-repulsion transition occurring in these excited states as discussed in [27]. This behavior also emerges in other quantities, such as E2 transition rates since the critical behavior of the initial or final states may be quite different from that of the ground state.

D. The isomer shift

Another quantity that is sensitive to the transition is the isomer shift defined by

$$\delta \langle r^2 \rangle = \alpha_0 (\langle 2_1^+; z | \hat{n}_d | 2_1^+; z \rangle - \langle 0_g^+; z | \hat{n}_d | 0_g^+; z \rangle), \quad (6)$$

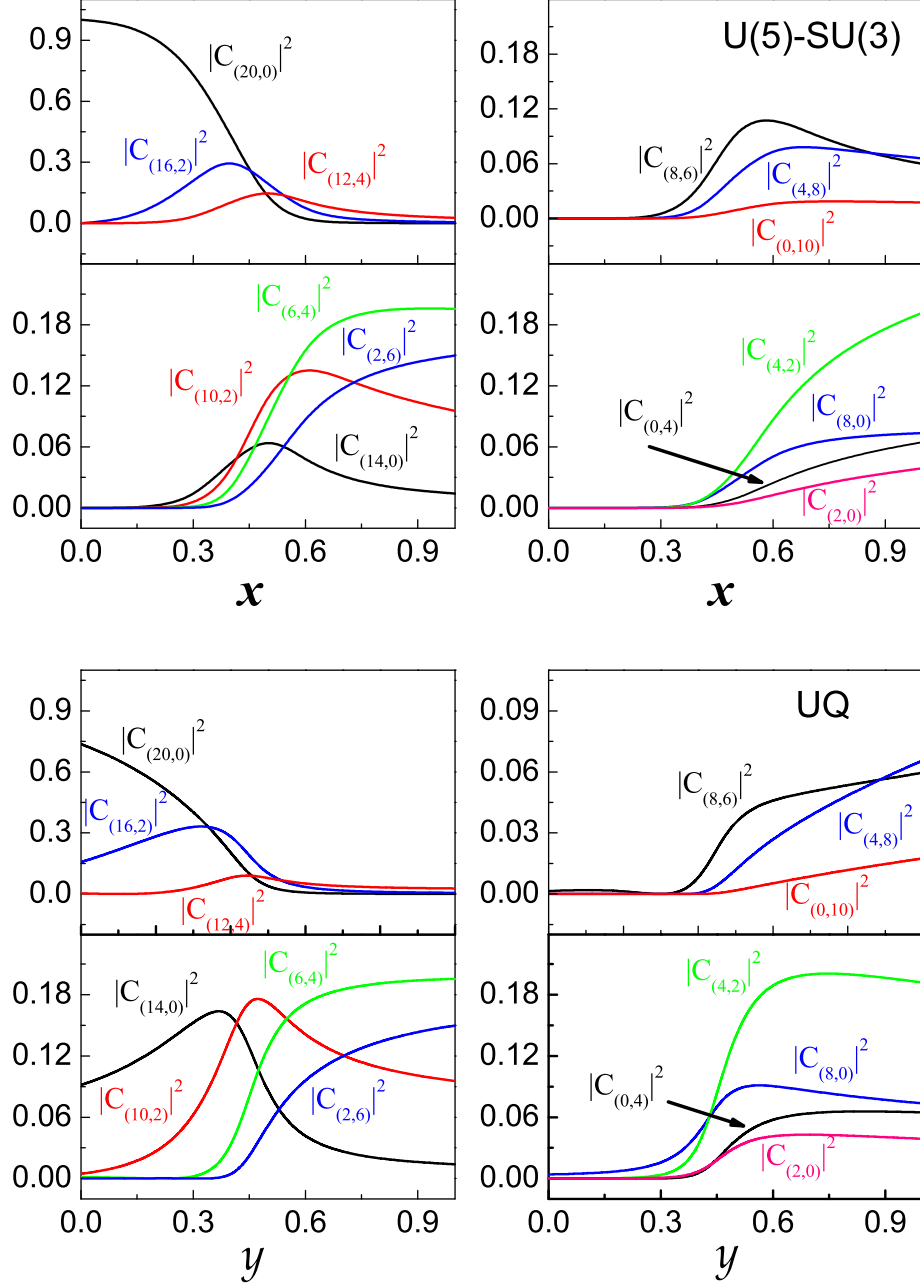


FIG. 3: (Color online) Amplitudes $|C_{(\lambda,\mu)}|^2$ in the ground state as function of the control parameter x for the $U(5)$ - $SU(3)$ case and y for the UQ scheme.

where α_0 is a constant. For the $U(5)$ - $SU(3)$ or the UQ schemes, the isomer shift as a function of transitional parameter $z = x$ or $z = y$ is shown in Fig. 6. In the $U(5)$ - $SU(3)$ scheme, the isomer shift ascends from 0.05 to 1.16. The largest absolute value of the derivative occurs around the critical point $x_c \sim 0.47$. There is a peak in the isomer shift at $x \sim 0.54$ in the $U(5)$ - $SU(3)$ scheme. Similar behavior also emerges in the UQ scheme. The isomer shift ascends rather precipitously from 0.09 to 1.28, the largest absolute value of the derivative of the isomer shift with respect to y also occurs around the critical point of $y_c \sim 0.48$. There is also a peak at $y \sim 0.52$ in the UQ scheme.

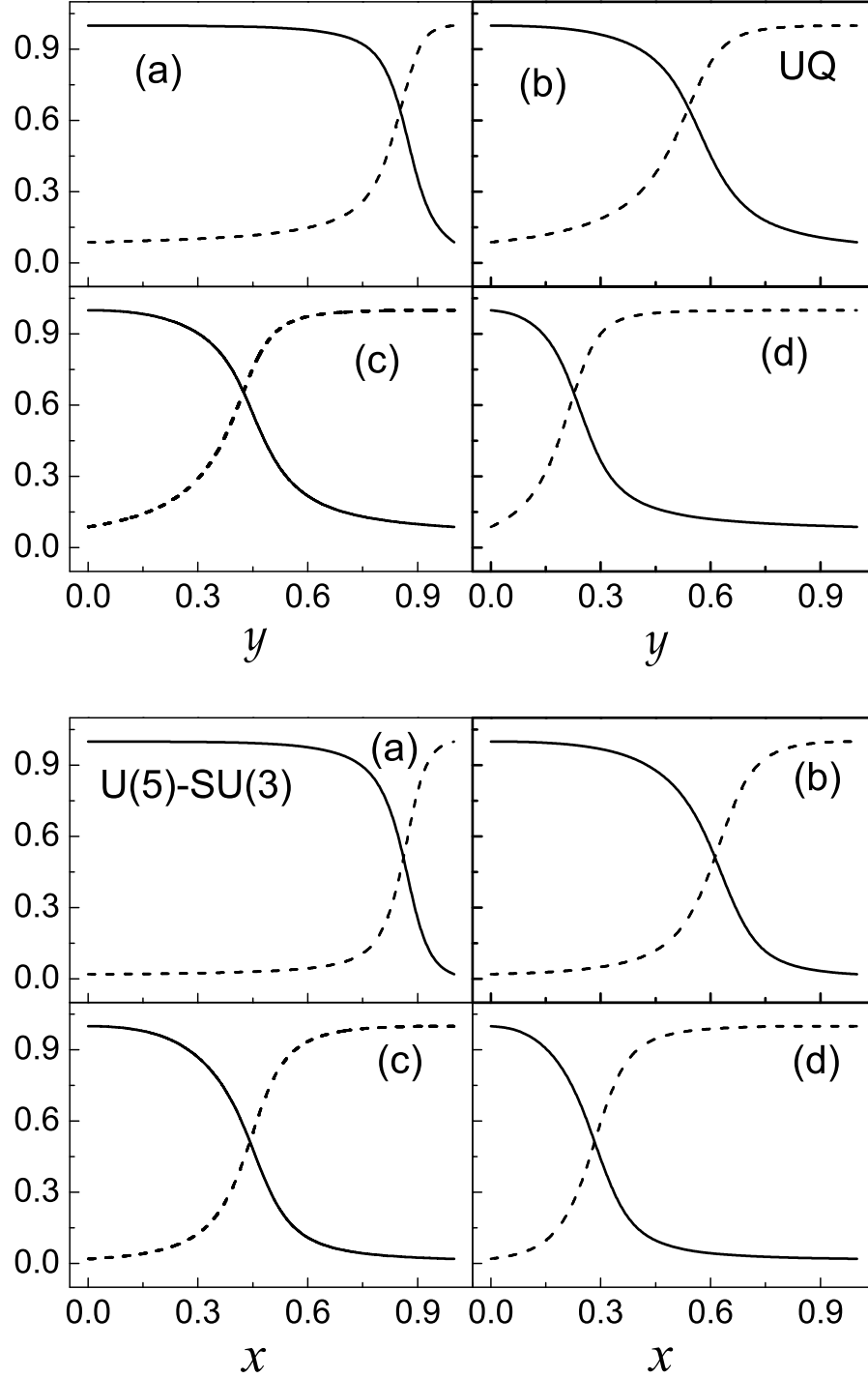


FIG. 4: Overlaps of the ground state, where the full line and dotted line show the overlaps $|\langle 0_g^+; z=0 | 0_g^+; z \rangle|$ and $|\langle 0_g^+; z=1 | 0_g^+; z \rangle|$, respectively, with $z = x$ in the $U(5)$ - $SU(3)$ scheme or $z = y$ in the UQ scheme. In the upper panel, (a) $f_1(N) = 0.5N$; (b) $f_1(N) = 2N$; (c) $f_1(N) = 4N$; (d) $f_1(N) = 8N$ for the $U(5)$ - $SU(3)$ scheme. In the lower panel, (a) $f_2(N) = 0.1N^2$; (b) $f_2(N) = 0.5N^2$; (c) $f_2(N) = 0.8N^2$; (d) $f_2(N) = 2N^2$ for the UQ scheme.

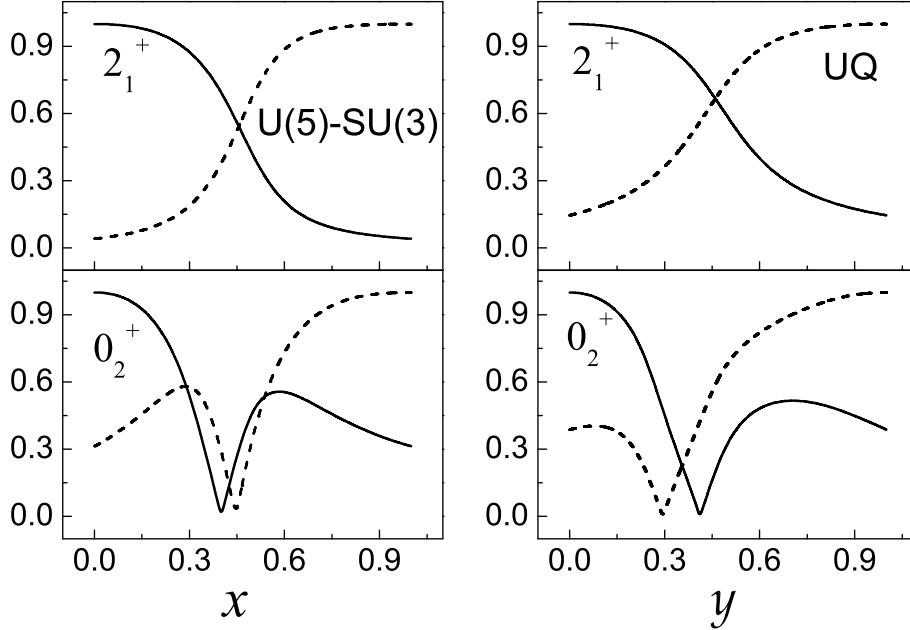


FIG. 5: Typical overlaps of two excited states, where the full line and dotted line show the overlap $|\langle L_\xi^+; z = 0 | L_\xi^+; z \rangle|$ and $|\langle L_\xi^+; z = 1 | L_\xi^+; z \rangle|$, respectively, with $z = x$ in the $U(5)$ - $SU(3)$ scheme shown in the left panel or $z = y$ in the UQ scheme shown in the right panel.

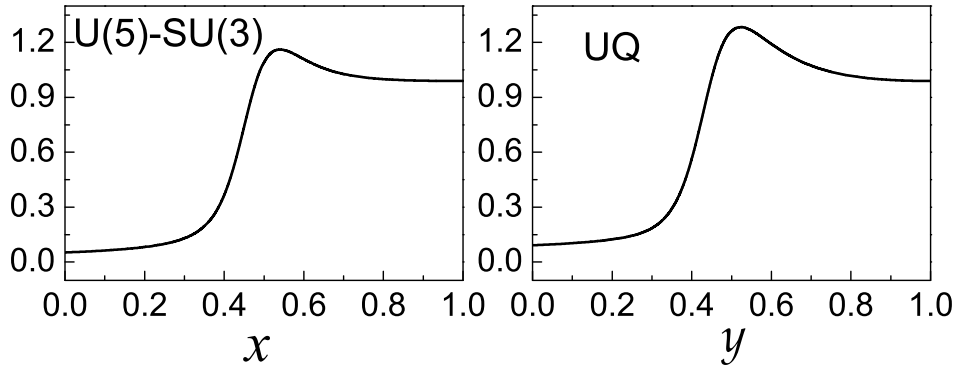


FIG. 6: The isomer shift $\delta(r^2)/\alpha_0$ as a function of the control parameter x in the $U(5)$ - $SU(3)$ scheme or y in the UQ scheme.

E. Some $B(E2)$ transitions

Another quantity that acts as a sensitive signature of the structure is $B(E2)$ transition. The $E2$ operator in the $U(5)$ - $SU(3)$ scheme is chosen the same as that used in [15] with

$$T_\mu(E2) = q_2 \hat{Q}_\mu(-\sqrt{7}/2), \quad (7)$$

where $\hat{Q}_\mu(-\sqrt{7}/2) = (s^\dagger \tilde{d}_\mu + d_\mu^\dagger s) - \sqrt{7}/2 (d^\dagger \tilde{d})_\mu^{(2)}$ are the $SU(3)$ generators, and q_2 is the effective charge. While in the UQ scheme, the $E2$ operator is chosen as

$$T_\mu(E2) = q_2 \hat{Q}_\mu(0), \quad (8)$$

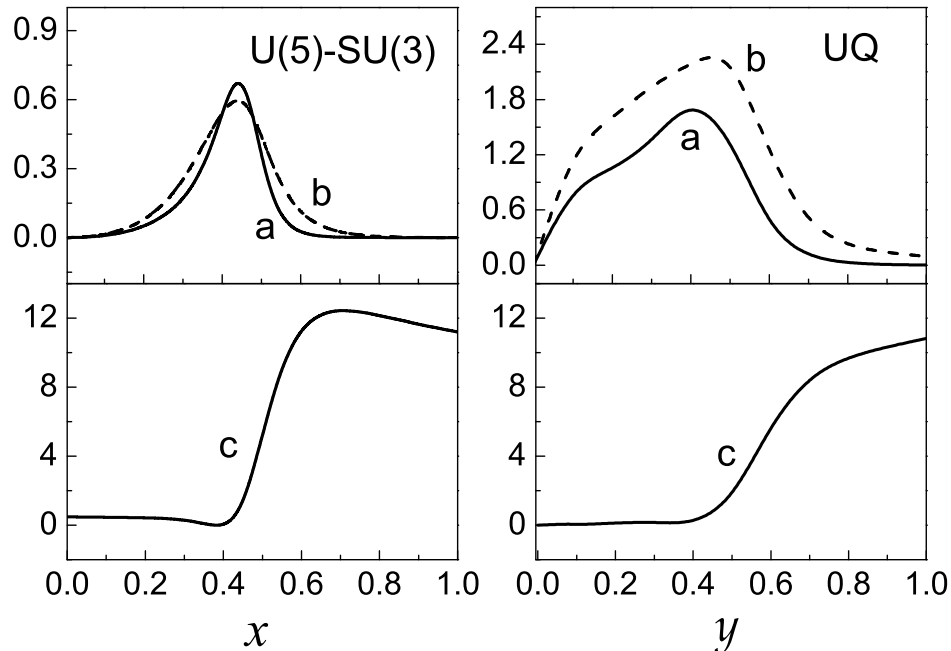


FIG. 7: $B(E2)/q_2^2$ values as functions of the control parameter x in the $U(5)$ - $SU(3)$ scheme (left panel) or y in the UQ scheme (right panel), where curve a represents $B(E2; 2_3^+ \rightarrow 0_g^+)/q_2^2$, curve b $B(E2; 2_3^+ \rightarrow 2_1^+)/q_2^2$, and curve c $B(E2; 2_3^+ \rightarrow 0_2^+)/q_2^2$.

where $\hat{Q}_\mu(0) = s^\dagger \tilde{d}_\mu + d_\mu^\dagger s$ are the $O(6)$ quadrupole operators.

Various $B(E2)$ values and ratios among the low-lying levels were studied in both schemes. Some $B(E2)$ values and ratios were found to be sensitive to the shape-phase transition. Three of these $B(E2)$ values are shown in Fig. 7. There is a small peak around $x \sim 0.45$ in the $B(E2; 2_3^+ \rightarrow 0_g^+)$ and the $B(E2; 2_3^+ \rightarrow 2_1^+)$ values in the $U(5)$ - $SU(3)$ scheme, and there is a small peak around $y \sim 0.43$ in the $B(E2; 2_3^+ \rightarrow 0_g^+)$ and around $y \sim 0.47$ in the $B(E2; 2_3^+ \rightarrow 2_1^+)$ of the UQ scheme. There is a saddle point around $x \sim 0.42$ in the $U(5)$ - $SU(3)$ scheme, and around $y \sim 0.43$ in the UQ scheme, respectively, in $B(E2; 2_3^+ \rightarrow 0_2^+)$. The peaks and saddle points in the $B(E2)$ values in both the $U(5)$ - $SU(3)$ and the UQ schemes are different from the critical point of the ground state. Fig. 8 shows six $B(E2)$ ratios for both the $U(5)$ - $SU(3)$ and the UQ schemes. And one can see that these ratios all undergo noticeable changes within the coexistence region. The most distinctive signature is shown by the $\frac{B(E2; 2_3^+ \rightarrow 0_1^+)}{B(E2; 2_3^+ \rightarrow 0_2^+)}$ curve d which has a giant peak around $x \sim 0.4$ in the $U(5)$ - $SU(3)$ scheme and $y \sim 0.42$ in the UQ scheme. This is mainly due to the near vanishing of the denominator $B(E2; 2_3^+ \rightarrow 0_2^+)$ factor as shown by curves c in in Fig. 7. However, the peaks in the $B(E2; 2_3^+ \rightarrow 0_g^+)$ and $B(E2; 2_3^+ \rightarrow 2_1^+)$ are not so sharp, with a larger width in the UQ scheme than in the $U(5)$ - $SU(3)$ scheme; and an increase in the $B(E2; 2_3^+ \rightarrow 0_2^+)$ with increasing z when $z \geq z_c$ is moderate in the UQ scheme, which indicates that the phase transition in the UQ scheme is smoother than for that of the $U(5)$ - $SU(3)$ scheme.

F. Nuclear shapes

It is well known that the Bohr variables (β, γ) are used to describe nuclear shape in the collective model. Though (β, γ) are not observable, theoretically, they can be used to estimate what nuclear shape looks like. The one-to-one relationship between the shape variables (β, γ) of the collective model and the $SU(3)$ irrep (λ, μ) in algebraic models was established in [28], which is used in this work to elucidate nuclear shape evolution during the transition [15]. In the $SU(3)$ algebraic approach, the Bohr variables β and γ can be expressed in terms of the second and third order Casimir operators of $SU(3)$ by

$$\hat{\beta} = \beta_0 \sqrt{\hat{C}_2(SU(3)) + 3} \quad (9)$$

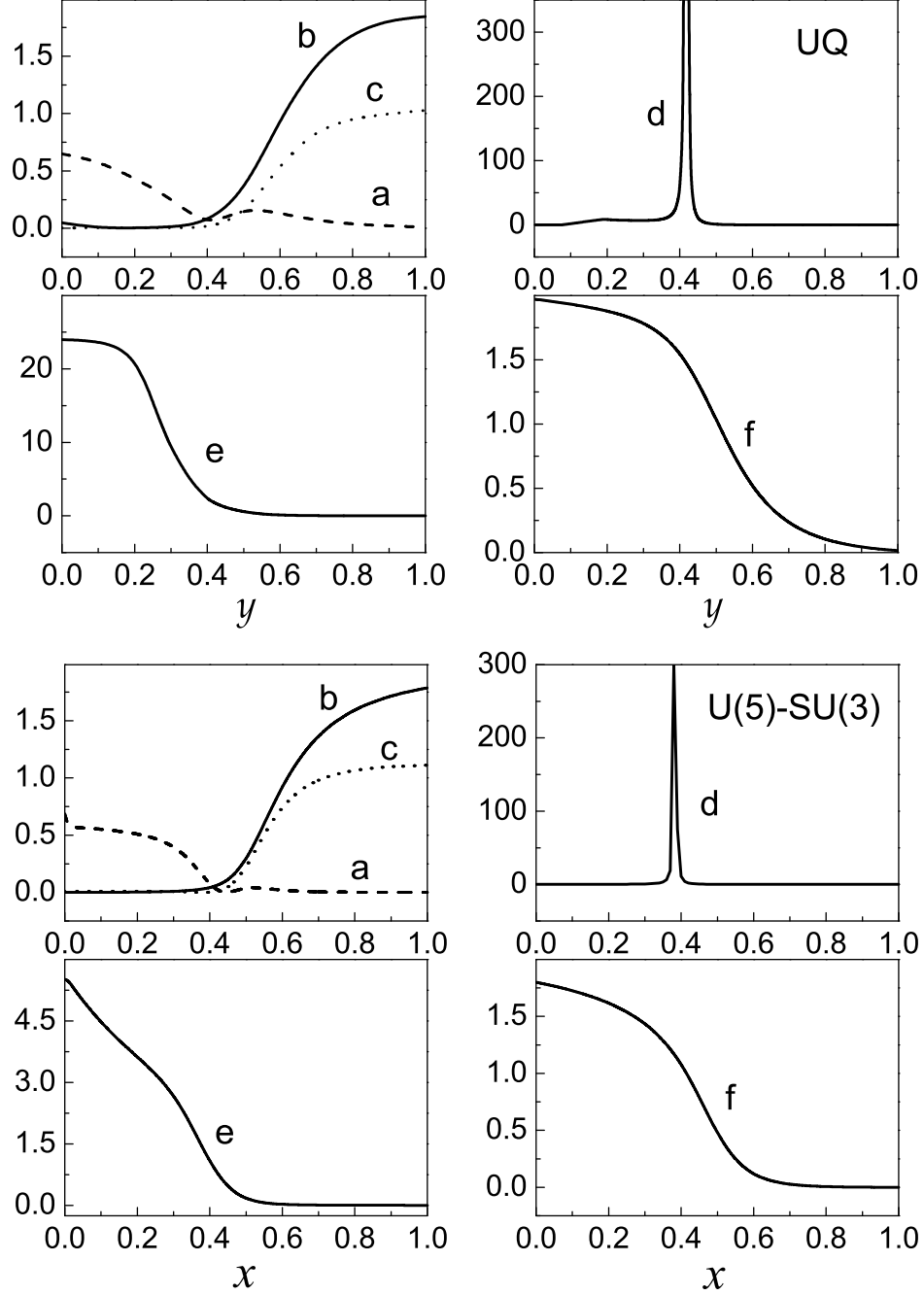


FIG. 8: Some B(E2) ratios as functions of the control parameter x in the $U(5)$ - $SU(3)$ scheme or y in the UQ scheme, where curves a , b , c , d , e , and f represent $\frac{B(E2;2_2^+ \rightarrow 0_1^+)}{B(E2;2_2^+ \rightarrow 2_1^+)}$, $\frac{B(E2;2_2^+ \rightarrow 2_1^+)}{B(E2;2_1^+ \rightarrow 0_1^+)}$, $\frac{B(E2;2_3^+ \rightarrow 0_2^+)}{B(E2;2_1^+ \rightarrow 0_1^+)}$, $\frac{B(E2;2_3^+ \rightarrow 0_1^+)}{B(E2;2_3^+ \rightarrow 0_2^+)}$, $\frac{B(E2;2_3^+ \rightarrow 2_1^+)}{B(E2;2_2^+ \rightarrow 2_1^+)}$, and $\frac{B(E2;3_1^+ \rightarrow 2_1^+)}{B(E2;3_1^+ \rightarrow 4_1^+)}$, respectively.

with

$$\beta_0 = \sqrt{\frac{4\pi}{5Ar_0^2}}, \quad (10)$$

where A is the number of like particles and r_0^2 is a dimensionless mean square radius [28], and

$$\hat{\gamma} = \tan^{-1}\left(\frac{\sqrt{3}(\hat{\mu} + 1)}{2\hat{\lambda} + \hat{\mu} + 3}\right), \quad (11)$$

where $\hat{\lambda}$ and $\hat{\mu}$ should be regarded as operators that take on the λ and μ values, respectively, when they act on the basis vector of $SU(3)$.

We then calculated the expectation value of $\hat{\beta}$ and $\hat{\gamma}$ in the ground state and the corresponding root mean square deviations defined by

$$\bar{\beta} = \langle 0_g^+; z | \hat{\beta} | 0_g^+; z \rangle, \quad (12)$$

$$\pm\Delta(\beta) = \pm\sqrt{\langle 0_g^+; z | (\hat{\beta} - \bar{\beta})^2 | 0_g^+; z \rangle}, \quad (13)$$

$$\bar{\gamma} = \langle 0_g^+; z | \hat{\gamma} | 0_g^+; z \rangle, \quad (14)$$

$$\pm\Delta(\gamma) = \pm\sqrt{\langle 0_g^+; z | (\hat{\gamma} - \bar{\gamma})^2 | 0_g^+; z \rangle}, \quad (15)$$

with $z = x$ in the $U(5)$ - $SU(3)$ scheme or $z = y$ in the UQ scheme. The expectation values $\bar{\beta}/\beta_0$ and $\bar{\gamma}$ of the ground state, and the corresponding root-mean-square deviations $\Delta(\beta)/\beta_0$ and $\Delta(\gamma)$ for the both schemes were calculated. The uncertainty in the shape variables as a function of the control parameter z can be seen in the results shown in Table I, Table II, and Fig. 9. In the $U(5)$ - $SU(3)$ scheme, it is obvious that $\Delta(\beta)$ and $\Delta(\gamma)$ are zero in the rotational limit ($x = 0$) that corresponds to a definite shape. In comparison to the $U(5)$ - $SU(3)$ scheme, one can see that $\Delta(\beta)$ and $\Delta(\gamma)$ in the UQ scheme are nonzero when $y = 0$, which should correspond to a superposition of different ellipsoid shapes. Thus, the shape is less well defined as x or y moves away from 0 either in the $U(5)$ - $SU(3)$ scheme or in the UQ scheme. The values of $\Delta(\beta)$ and $\Delta(\gamma)$ are all not small in the vibrational limit ($x = 1$ or $y = 1$) in the two schemes due to the quadrupole vibration being non-negligible. The fluctuations in γ remain fairly large and constant after the critical point in the both schemes may be explained in the following way: When the system is spherical, all γ values are possible in the sense that the corresponding periodic wave function in γ is not concentrated around a small interval but covers the full wedge, which means that the fluctuations will be rather large because of γ -instability. As can be seen from Fig. 9, there are also obvious changes in $\bar{\beta}$ and $\bar{\gamma}$ in the critical region around $x_c = 0.47$ in the $U(5)$ - $SU(3)$ scheme or $y_c = 0.48$ in the UQ scheme. Over the whole range, the magnitude of the change in $\bar{\gamma}$ is small. From Table I and Table II, it can be seen that $\Delta(\beta)$ reaches the maximum value at $x = 0.5$ in the $U(5)$ - $SU(3)$ scheme or $y = 0.45$ in the UQ scheme, in which the critical point value deviates only slightly from the critical point $x_c \sim 0.47$ or $y_c \sim 0.48$ in the ground state, but is still near the corresponding critical point. This distinctive signature shows that nucleus is the softest in the critical region. This fact can help us to understand why there is a saddle region in most excited levels shown in Fig. 1. As a consequence, a nucleus that lies near the critical point can be easily excited, which results in relatively smaller energy gaps in this soft critical region. The results also indicate that both the $U(5)$ - $SU(3)$ and the UQ schemes can be used to describe nuclei within the spherical to axially deformed transitional region, with results near the critical point that are quite similar.

G. E2 transitions in the deformed limit

Besides the transition from the spherical to the deformed shape phase in the UQ scheme is considerably smoother than that in the $U(5)$ - $SU(3)$ scheme, there are some notable differences between the spectrum in the UQ scheme and

TABLE I: Expectation values $\bar{\beta}/\beta_0$ and $\bar{\gamma}$ of the ground state, and the corresponding root-mean-square deviations $\Delta(\beta)/\beta_0$ and $\Delta(\gamma)$ for some specific values of the control parameter x in the $U(5)$ - $SU(3)$ scheme (left) and y in the UQ scheme (right).

$\Delta(\gamma)$	$\bar{\gamma}$	$\Delta(\beta)/\beta_0$	$\bar{\beta}/\beta_0$	$x(y)$	$\bar{\beta}/\beta_0$	$\Delta(\beta)/\beta_0$	$\bar{\gamma}$	$\Delta(\gamma)$
0.000	0.040	0.003	21.517	0.0	20.382	2.158	0.060	0.046
0.012	0.042	0.357	21.473	0.1	20.074	2.321	0.067	0.049
0.029	0.049	0.835	21.273	0.2	19.574	2.584	0.077	0.054
0.054	0.068	1.527	20.711	0.3	19.671	3.053	0.096	0.067
0.110	0.123	2.726	19.070	0.4	16.410	4.126	0.151	0.124
0.208	0.283	3.873	14.787	0.5	12.124	4.384	0.298	0.214
0.230	0.390	3.503	12.040	0.6	10.408	3.636	0.381	0.232
0.234	0.428	3.239	10.952	0.7	9.939	3.279	0.417	0.235
0.235	0.445	3.100	10.373	0.8	9.789	3.107	0.437	0.236
0.236	0.454	3.012	10.005	0.9	9.744	3.012	0.450	0.237
0.237	0.460	2.953	9.74	1.0	9.747	2.953	0.460	0.237

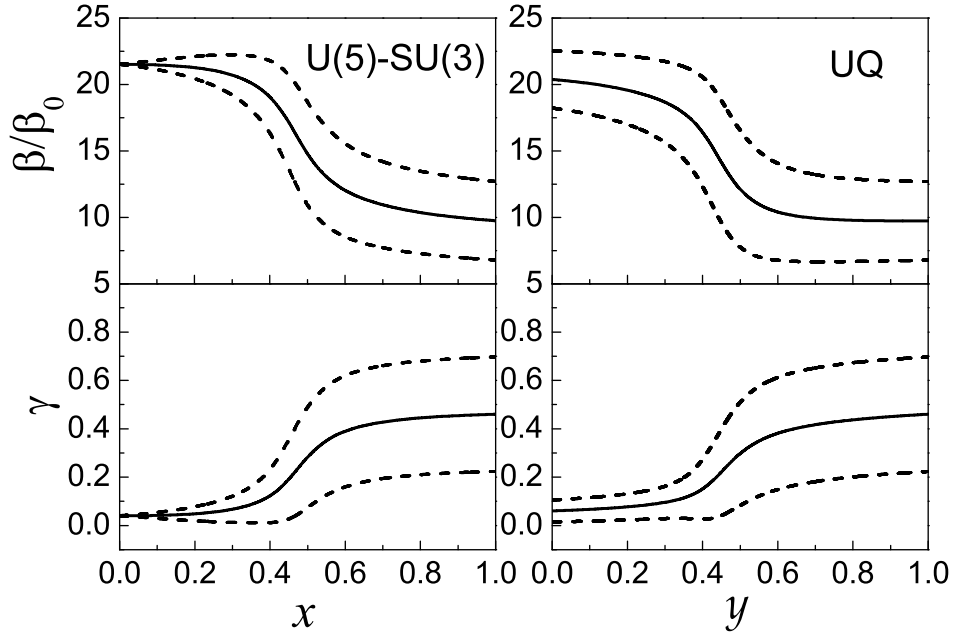


FIG. 9: The ground state expectation values of Bohr variables $\bar{\beta}/\beta_0$ and $\bar{\gamma}$ and the corresponding root mean square deviations $\Delta\bar{\beta}/\beta_0$ and $\Delta\bar{\gamma}$, where the full line indicates the expectation value $\bar{\beta}/\beta_0$ or $\bar{\gamma}$, while the dotted lines show the corresponding root mean square deviations $\pm\Delta\bar{\beta}/\beta_0$ or $\pm\Delta\bar{\gamma}$. The left (right) panel shows results of the $U(5)$ - $SU(3)$ (UQ) scheme.

that in the $U(5)$ - $SU(3)$ scheme in the deformed limit as shown in [18]. Specifically, in the $U(5)$ - $SU(3)$ scheme with $x = 0$, the β and γ bands belong to the same $SU(3)$ representation, are degenerate in energy, and are connected by strong E2 transitions, while in the UQ scheme, in contrast, the “ β ” and γ band belong to different $O(6)$ representations. Thus, E2 transition from the β to the γ band or vice versa in the UQ scheme with $y = 0$ is forbidden. In addition to the different E2 selection rules between the β and γ band already shown in [18], we also calculated inter-band transitions from β or γ band to the ground band for both schemes with $N = 10$. Some low-lying states in the ground, the β , and γ bands in the two schemes, together with intra-band transitions and inter-band transitions from the β or γ band to the ground band, are shown in Fig. 10. It is shown in Fig. 10 that the corresponding intra-band E2 transition rates of the two schemes are almost the same. Since the E2 operator is chosen as the $SU(3)$ generators according to (7) in the $U(5)$ - $SU(3)$ scheme, the inter-band transitions from the β or γ band to the ground band is forbidden, while they are allowed in the UQ scheme, though these inter-band E2 transition rates are considerably smaller than those of the intra-bands.

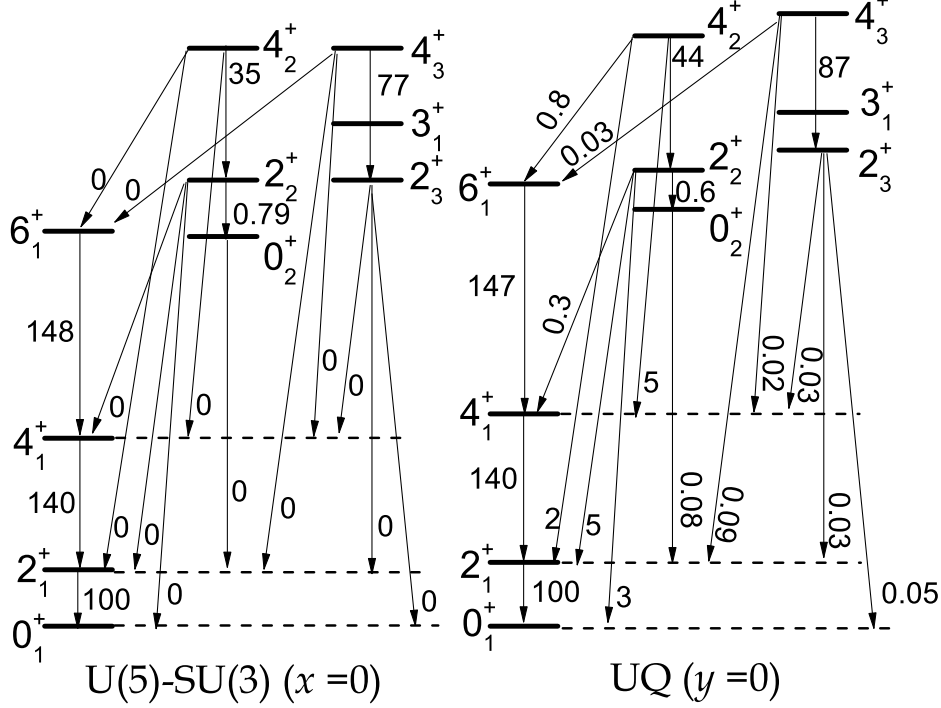


FIG. 10: Some Low-lying inter-band and intra-band E2 transitions in the $U(5)$ - $SU(3)$ scheme with $x = 0$ and in the UQ scheme with $y = 0$, where the effective charge is normalized with $B(E2, 2_1^+ \rightarrow 0_1^+) = 100$. The inter-band transitions between β and γ band discussed in [18] are not shown.

H. Low-lying spectrum of ^{152}Sm

In order to demonstrate that the UQ scheme indeed serves as an alternative description of the spherical to axially deformed phase transition, in this subsection, the possible $X(5)$ critical point symmetry candidate ^{152}Sm is taken as an example to be described by the UQ scheme, of which the results are compared with the experimental data and those obtained from the $U(5)$ - $SU(3)$ scheme. In Table II, the experimental data [29, 31, 32] and the calculated results from both the $U(5)$ - $SU(3)$ and the UQ scheme, which include low-lying excitation energies $E(L^+)$ (in keV) normalized to the 2_1^+ state, quadrupole moment Q (in eb) of the 2_1^+ state and $B(E2)$ values (in W.u.) normalized to the $2_1^+ \rightarrow 0_1^+$ transition, and the corresponding mean-square deviation $\sigma(E)$ (in keV) defined by $\sigma(E) = \sqrt{\sum_i^{\mathcal{N}} |E_{exp}^i - E_{th}^i|^2 / \mathcal{N}}$ for excitation energies or $\sigma(BE2)$ (in W.u) by $\sigma(BE2) = \sqrt{\sum_i^{\mathcal{N}} |BE(2)_{exp}^i - BE(2)_{th}^i|^2 / \mathcal{N}}$ for $B(E2)$ values, where \mathcal{N} is the total number of excitation energies in $\sigma(E)$ (or transitions in $\sigma(BE2)$) fitted. $B(E2)$ results calculated from other models, such as $X(5)$ model [13], the (Bohr) collective model [30], and $X^*(5)$ model [31], are also shown. It shows from Table II that the overall fitting quality of the UQ scheme for both the excitation energies and the $BE(2)$ values is better than that of the $U(5)$ - $SU(3)$ scheme. As far as E2 transition rates are concerned, the modified $X^*(5)$ model [31] seems better.

Fig. 11 shows some typical $B(E2)$ values calculated from the $U(5)$ - $SU(3)$ and the UQ schemes and the corresponding experimental results of ^{152}Sm , where (a), (b), (c), and (d) represent $B(E2; 4_1^+ \rightarrow 2_1^+)$, $B(E2; 0_2^+ \rightarrow 2_1^+)$, $B(E2; 4_2^+ \rightarrow 6_1^+)$, and $B(E2; 2_3^+ \rightarrow 4_1^+)$, respectively. It is clearly shown in Fig. 11 that the transition rate within the ground band, $B(E2; 4_1^+ \rightarrow 2_1^+)$, calculated from the both schemes is almost the same, while the inter band transitions between the β or γ band and the ground band calculated from the two schemes are quite different, in which the three transition rates, $B(E2; 0_2^+ \rightarrow 2_1^+)$, $B(E2; 4_2^+ \rightarrow 6_1^+)$, and $B(E2; 2_3^+ \rightarrow 4_1^+)$, calculated from the $U(5)$ - $SU(3)$ scheme are too large in comparison to the corresponding experimental results. The results show that the UQ scheme is better than the $U(5)$ - $SU(3)$ scheme in fitting both the inter-band and the intra-band E2 transitions.

TABLE II: The experimental data (Exp.) [29, 31, 32] and calculated results from both the $U(5)$ - $SU(3)$ and the UQ schemes for ^{152}Sm , including low-lying excitation energies $E(L^+)$ (in keV) normalized to the 2_1^+ state, quadrupole moment $Q(2_1^+)$ (in eb) and $B(E2)$ values (in W.u.) normalized to the $2_1^+ \rightarrow 0_1^+$ transition, and $B(E2)$ values calculated from the X(5) [13], Bohr [30], and X*(5) [31]. The corresponding mean-square deviations are also provided. “-” denotes the corresponding value was not calculated previously, which is not included in the corresponding mean-square deviation $\sigma(BE2)$.

$E(L^+)$	2_1^+	4_1^+	6_1^+	8_1^+	10_1^+	0_2^+
Exp.	122	366	707	1125	1609	685
$U(5)$ - $SU(3)$	122	316	575	893	1267	379
UQ	122	340	645	1020	1445	369
	2_2^+	4_2^+	6_2^+	8_2^+	2_3^+	3_1^+
Exp.	810	1023	1311	1666	1086	1234
$U(5)$ - $SU(3)$	580	857	1179	1549	739	898
UQ	676	1011	1374	1758	931	1076
	4_3^+	5_1^+	6_3^+	7_1^+	$\sigma(E)$	$Q(2_1^+)$
Exp.	1372	1560	1728	1946		-1.702
$U(5)$ - $SU(3)$	1062	1203	1416	1556	255	-1.680
UQ	1224	1354	1568	1686	149	-1.713
$L_i^+ \rightarrow L_f^+$	B(E2)					
	Exp.	$U(5)$ - $SU(3)$	UQ	X(5)	Bohr	X*(5)
$2_1^+ \rightarrow 0_1^+$	144	144	144	144	144	144
$4_1^+ \rightarrow 2_1^+$	209	235.64	225.57	230.40	230	216
$6_1^+ \rightarrow 4_1^+$	245	273.93	254.49	285.12	285	249.12
$8_1^+ \rightarrow 6_1^+$	285	287.78	264.04	328.32	328	267.84
$10_1^+ \rightarrow 8_1^+$	320	284.33	261.21	361.44	361	279.36
$2_2^+ \rightarrow 0_2^+$	111	92.91	73.80	115.2	114	109.44
$4_2^+ \rightarrow 2_2^+$	204	147.18	122.85	172.8	173	161.28
$0_2^+ \rightarrow 2_1^+$	32.7	128.99	66.53	90.72	83	36
$2_2^+ \rightarrow 0_1^+$	0.92	0.36	0.46	3.02	3	0.004
$2_2^+ \rightarrow 2_1^+$	3	24.23	11.86	11.95	11	2.02
$2_2^+ \rightarrow 4_1^+$	19	31.35	14.69	53.28	49	20.74
$4_2^+ \rightarrow 2_1^+$	1.20	0	0.038	1.44	1	1
$4_2^+ \rightarrow 4_1^+$	5	16.07	13.80	9.07	8	0.86
$4_2^+ \rightarrow 6_1^+$	4	20.41	5.61	40.32	37	12.82
$2_3^+ \rightarrow 0_1^+$	3.62	3.13	15.32	14.69	-	8.93
$2_3^+ \rightarrow 2_1^+$	9.30	2.98	18.33	22.32	-	13.39
$2_3^+ \rightarrow 4_1^+$	0.78	14.60	5.88	1.17	-	0.66
$4_3^+ \rightarrow 6_1^+$	1.20	11.52	10.60	-	-	-
$4_3^+ \rightarrow 2_1^+$	0.59	0.85	5.78	9.79	-	5.62
$4_3^+ \rightarrow 4_1^+$	5.50	1.95	15.24	31.25	-	17.42
$4_3^+ \rightarrow 2_2^+$	0.18	1.35	2.39	1.20	-	0.29
$4_3^+ \rightarrow 2_3^+$	50	85.12	70.51	95.04	-	89.28
$\sigma(BE2)$		28.79	25.62	27.33	28.21	16.48

IV. CONCLUSION

The quantum phase transitional behavior of a new scheme for the description of the spherical to axially deformed shape-phase transition in the interacting boson model has been analyzed, where the $SU(3)$ quadrupole-quadrupole interaction is replaced by the $O(6)$ cubic interaction. In order to compare the quantum phase transitional behavior of the new scheme with that of the $U(5)$ - $SU(3)$ transitional description, the low-lying energy levels, eigenstates, amplitudes $|C_{(\lambda,\mu)}|^2$ in the ground state and overlap of the ground state, overlaps of two typical excited states, the isomer shifts, E2 transition rates, and expectation values of the ground state shape variables across the entire transitional

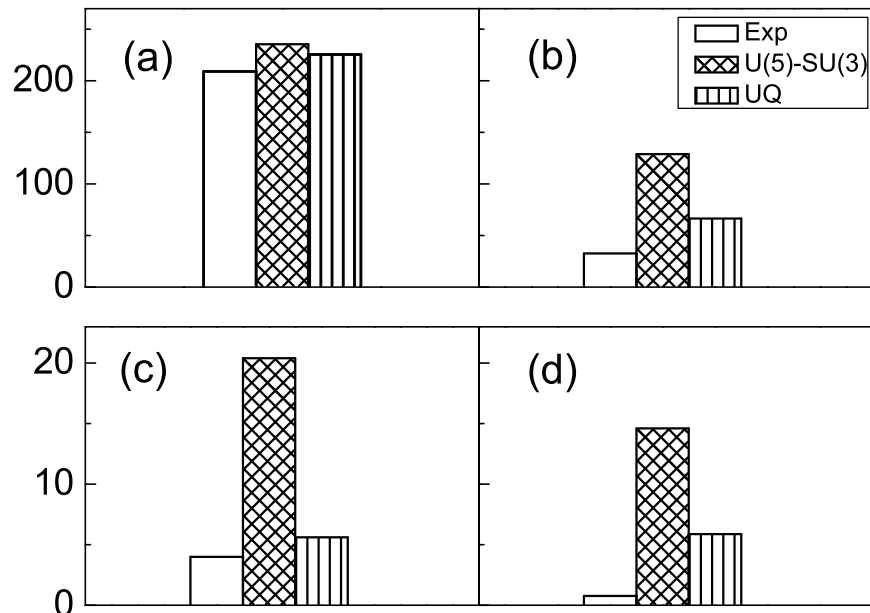


FIG. 11: $B(E2)$ values calculated from the $U(5)$ - $SU(3)$ and the UQ schemes and the corresponding experimental data of ^{152}Sm , where (a), (b), (c), and (d) represent $B(E2; 4_1^+ \rightarrow 2_1^+)$, $B(E2; 0_2^+ \rightarrow 2_1^+)$, $B(E2; 4_2^+ \rightarrow 6_1^+)$, and $B(E2; 2_3^+ \rightarrow 4_1^+)$, respectively.

region as functions of the control parameter for a finite N case has been analyzed. Although the transitional behavior of the two schemes was found to be quite similar, there are some quite distinctive differences for some quantities across the entire transitional region, such as energy levels and ratios, eigenstates, $B(E2)$ values and ratios, and expectation values of the shape variables. Generally speaking, the transition is smoother in the new scheme with a replacement of the $SU(3)$ quadrupole-quadrupole interaction by the $O(6)$ cubic interaction, a results that a similar analysis in the large- N limit is expected to confirm.

In addition, we found that, in contrast to the situation in the $U(5)$ - $SU(3)$ description, the nuclear shape in the new scheme is less well defined even in the “axially deformed” limit. As widely accepted, nuclei in the axially deformed limit should be quite rigid. But nuclei described in the new scheme are not so rigid with non-negligible $\Delta(\beta)$ and $\Delta(\gamma)$ even in the “axially deformed” limit. This is due in the main to the replacement of the $SU(3)$ quadrupole-quadrupole interaction by the $O(6)$ cubic interaction. As is well known, the $O(6)$ symmetry is suitable to describe γ -unstable motion, which may come into play when the $O(6)$ cubic interaction is adopted, though the fluctuation $\Delta(\gamma)$ is small in this case. With increasing value of the control parameter, namely near the critical point of the spherical to axially deformed shape-phase transition, the transitional behavior of the two schemes seems quite similar, though the transition is smoother in the new scheme. And indeed, as shown in the application of the two schemes to the critical point symmetry candidate, ^{152}Sm , together with our recent application of the new scheme in a description of the ^{150}Nd and ^{154}Gd nuclei, which are all near the X(5) critical point [33], there is little difference in excitation energies for the two schemes, but the overall fitting quality of the UQ scheme is better than that of the $U(5)$ - $SU(3)$ scheme, especially for the inter-band E2 transitions in ^{152}Sm . As has been stated in [18], whether the cubic interaction in place of the usual quadrupole-quadrupole interaction is required in the deformed limit is not clear at the moment since comprehensive phenomenological studies of this question are lacking. Nevertheless, the spectrum generated by the cubic interaction has many of the properties that are typical of deformed nuclei. More importantly, as shown in this work, the overall fitting quality of the new scheme is better than that of the usual $U(5) - SU(3)$ scheme when they are applied to describe nuclei near the critical point.

Acknowledgments

Support from the U.S. National Science Foundation (OCI-0904874), the Southeastern Universities Research Association, the Natural Science Foundation of China (10975068 & 11175078), the Doctoral Program Foundation of the State Education Ministry of China (20102136110002), the Project of Knowledge Innovation Program (PKIP) of Chinese Academy of Sciences, Grant No. KJJCX2.YW.W10, and the LSU–LNNU joint research program (9961) is acknowledged.

-
- [1] S. Sachdev, *Quantum Phase Transitions* (Cambridge Univ. Press, Cambridge, 1999)
 - [2] D. J. Rowe, G. Thiamova, *Nucl. Phys. A* **760** (2005) 59.
 - [3] G. Thiamova, *Eur. Phys. J. A* **45** (2010) 81.
 - [4] L. Fortunato, C. E. Alonso, J. M. Arias, J. E. García-Ramos, and A. Vitturi, *Phys. Rev. C* **84** (2011) 014326.
 - [5] A. Arima and F. Iachello, *Ann. Phys. (N.Y.)* **99** (1976) 253.
 - [6] A. Arima and F. Iachello, *Ann. Phys. (N.Y.)* **111** (1978) 201.
 - [7] A. Arima and F. Iachello, *Ann. Phys. (N.Y.)* **123** (1979) 468.
 - [8] R. F. Casten, in: F. Iachello (Ed.), *Interacting Bose-Fermi System* (Plenum, New York, 1981).
 - [9] A. E. L. Dieperink, O. Scholten, and F. Iachello, *Phys. Rev. Lett.* **44** (1980) 1747.
 - [10] A. E. L. Dieperink and O. Scholten, *Nucl. Phys. A* **346** (1980) 125.
 - [11] D. H. Feng, R. Gilmore, and S. R. Deans, *Phys. Rev. C* **23** (1981) 1254.
 - [12] O. Scholten, F. Iachello, and A. Arima, *Ann. Phys. (N.Y.)* **115** (1978) 325.
 - [13] F. Iachello, *Phys. Rev. Lett.* **87** (2001) 052502.
 - [14] R. F. Casten and N. V. Zamfir, *Phys. Rev. Lett.* **87** (2001) 052503.
 - [15] F. Pan, J. P. Draayer, and Y. Luo, *Phys. Lett. B* **576** (2003) 297.
 - [16] G. Rosensteela, D. J. Rowe, *Nucl. Phys. A* **759** (2005) 92.
 - [17] R. Fossion, C. E. Alonso, J. M. Arias, L. Fortunato, and A. Vitturi, *Phys. Rev. C* **76** (2007) 014316.
 - [18] P. van Isacker, *Phys. Rev. Lett.* **83** (1999) 4269
 - [19] G. Thiamova and P. Cejinar, *Nucl. Phys. A* **765** (2006) 97.
 - [20] D. D. Warner and R. F. Casten, *Phys. Rev. C* **28** (1983) 1798.
 - [21] V. Werner, P. von Brentano, R. F. Casten, and J. Joile, *Phys. Lett. B* **527** (2002) 55.
 - [22] J. P. Draayer and Y. Akiyama, *J. Math. Phys.* **14** (1973) 1904.
 - [23] Y. Akiyama and J. P. Draayer, *Comput. Phys. Commun.* **5** (1973) 405.
 - [24] G. Rosensteel, *Phys. Rev. C* **41** (1990) 730.
 - [25] D. J. Rowe, P. S. Turner and G. Rosensteel, *Phys. Rev. Lett.* **93** (2004) 232502.
 - [26] D. J. Rowe, *Phys. Rev. Lett.* **93** (2004) 122502.
 - [27] F. Pan, T. Wang, Y.-S. Huo, and J. P. Draayer, *J. Phys. G* **35** (2008) 125105.
 - [28] O. Castaños, J. P. Draayer, and Y. Leschber, *Z. Phys. A* **329** (1988) 33.
 - [29] R. Krücken, B. Albanna, C. Bialik, R. F. Casten, J. R. Cooper, A. Dewald, N. V. Zamfir, C. J. Barton, C. W. Beausang, M. A. Caprio, A. A. Hecht, T. Klug, J. R. Novak, N. Pietralla, and P. von Brentano, *Phys. Rev. Lett.* **88** (2002) 232501.
 - [30] P. G. Bizzeti and A. M. Bizzeti-Sona, *Phys. Rev. C* **81** (2010) 034320.
 - [31] R. V. Jolos and P. von Brentano, *Phys. Rev. C* **80** (2009) 034308.
 - [32] Y. Yamazaki, E. B. Shera, and M. V. Hoehn, *Phys. Rev. C* **18** (1978) 1474.
 - [33] L.-R. Dai, W.-X. Teng, F. Pan, and S.-H. Wang, *Chin. Phys. Lett.* **28** (2011) 052101.